JMEPEG (2014) 23:3285–3298
DOI: 10.1007/s11665-014-1109-2

1059-9495/$19.00

Corrosion Behavior of 9Cr-1Mo Steel in Sulfur Dioxide Environment

V. Singh, J.S. Kachhawaha, and V.B. Tare

(Submitted June 3, 2013; in revised form March 20, 2014; published online June 27, 2014)

Corrosion behavior of annealed 9Cr-1Mo steel was studied in SO_2 environment at 1173 K, at flow rates from 8.33×10^{-7} to 33.33×10^{-7} m^3/s, and parabolic rate law was followed. The rate constants were found to be independent of flow rate, within the range of flow rate investigated. Corrosion at temperatures from 973 to 1173 K, at a constant flow rate of 16.66×10^{-7} m^3/s, at 1 atmospheric pressure, for 6 h also exhibited parabolic law, however, the rate constants were observed to increase significantly with rise in temperature. The outer layer of the scale formed at 973 K was essentially of iron oxide, with small amount of chromium oxide whereas the inner layer was predominantly of chromium sulphide and chromium oxide. The scale formed at 1173 K was multilayered, in contrast to double layered formed at 973 K and 1073 K. The outer thick layer of the scale formed at 1173 K, consisted of iron oxide followed by thin substrate of chromium sulphide, iron sulphide/iron oxide, and chromium sulphide/chromium oxide toward the substrate. A model is proposed for the process of corrosion of 9Cr-1Mo steel in SO_2 environment, based on the present investigation.

Keywords activation energy, corrosion, 9Cr-1Mo steel, SO_2 environment

1. Introduction

Metals and alloys are exposed to multi component gaseous environments at elevated temperature in many industrial applications such as in gas turbine engines, coal conversion systems, boilers etc. In these cases, the atmosphere usually consists of oxygen, nitrogen, hydrocarbons, and sulfur compounds. Corrosion of metals and alloys under such atmospheres is a complex phenomenon and understanding of the mechanism of corrosion is important as these oxidants strongly affect the rate of corrosion. For example, the rate of corrosion of nickel in mixed SO_2-O_2 environment is increased by 10^5 to 10^6 times than that in air (Ref 1). The understanding of the kinetics and mechanism of scaling becomes more difficult in case of alloys than that of pure metals in gaseous environment containing more than one oxidant.

In order to understand the process of reactions in such complex systems the kinetics and the mechanism of the reaction of a pure metal with SO_2 in general and simultaneous oxidation and sulfidation in particular is essential. This aspect has been extensively studied because of the following reasons.

1. Growing interest in coal gasification or geothermal application in which sulfur is one of the major constituents of the atmospheres apart from oxygen (Ref 2).
2. Need for prevention of corrosion of structural materials of combustion engines using fossil fuel, containing sulfur as a major impurity (Ref 3).
3. Sulfides and oxides, as reaction products in simultaneous oxidation and sulfidation, tend to increase the rate of corrosion compared to that of pure oxidation, because sulfides usually have lower melting points than those of oxides and often form low melting eutectics with metals or metal oxides (Ref 4).

However, the understanding of the mechanism of corrosion of metals and alloys in binary oxidants is yet far from complete and it is difficult to make clear predictions on behavior of materials exposed to corresponding atmospheres. These difficulties arise not only from the fact that phases which are thermodynamically unstable with respect to the bulk gas composition are formed due to various kinetic reasons (Ref 5).

Solubility of sulfur in oxide depends on temperature as well as the pressure of sulfur in the gas phase. On cooling, sulfide may precipitate in the oxide because the solubility of sulfur decreases with decrease in temperature. In this case, formation of oxide and sulfide is not really simultaneous. Although there are definite evidences that sulfur can be dissolved in certain metal oxides. It seems that solubility of sulfur in the oxides such as FeO, Fe_3O_4, Cu_2O, and NiO is too small to account for the amount of sulfides found in the scale (Ref 1, 5, 6).

When metals such as Fe (Ref 6-8), Co (Ref 9), or Ni (Ref 1, 10) are exposed to oxygen-sulfur containing gas, metal sulfides have been found underneath the oxide scale even when only oxides are stable with respect to the bulk gas compositions. For

V. Singh, Department of Metallurgical Engineering, Center of Advanced Study, Indian Institute of Technology (Banaras Hindu University), Varanasi 221005 UP, India and Department of Mechanical Engineering, Padmashree Dr. D.Y. Patil Institute of Engineering and Technology, Pimpri, Pune 411018 Maharashtra, India; and **J.S. Kachhawaha** and **V.B. Tare**, Department of Metallurgical Engineering, Center of Advanced Study, Indian Institute of Technology (Banaras Hindu University), Varanasi 221005 UP, India. Contact e-mail: vsinghdr@rediffmail.com.

Table 1 Chemical composition of the 9Cr-1Mo steel used (in wt.%)

C	Si	Mn	S	P	Cr	Mo	Nb	Al	V
0.10	0.26	0.35	0.02	0.025	8.48	0.90	0.09	0.013	0.21

sulfide to be formed underneath the oxide scale, sulfur or sulfur containing gas species must be transported through the oxide scale to the metal/scale interface. There are two modes of sulfur transportation through the oxide scale.

(a) Dissolution and diffusion of sulfur as a lattice constituent.
(b) Transport as gas species S_2, SO_2 or SO_3 molecules through microcracks, grain boundaries, or dislocation pipes.

These two mechanisms of transport may proceed at the same time in actual scaling processes.

Kor (Ref 11) considered the mechanism of sulfur transport through lattice diffusion and observed that diffusion coefficient of sulfur in FeO was very high and was of the same order of magnitude as that of Fe in FeO in equilibrium with iron. High diffusion coefficients have also been reported for diffusion of sulfur in Cr_2O_3 (Ref 12). Role of lattice diffusion of sulfur in influencing overall kinetics of corrosion is required to be considered along with transport of sulfur by alternate routes.

Further, work related to enhancement of corrosion rate due to SO_2 has been carried out in simulated combustion fuel atmosphere (Ref 13). The effect of partial pressure of SO_2 on the rate of corrosion of pure iron at elevated temperatures was first studied by Flately and Birks (Ref 8). They observed that pure iron oxidized according to a linear rate law for the first few minutes and subsequently there was a parabolic rate law. Chatterjee and Dowell (Ref 14) have also reported oxidation of pure iron in SO_2 gas at one atmospheric pressure, in the temperature range 973-1173 K, obeying a parabolic law. Similar results are reported by Rahmel and Gonzalez (Ref 15, 16). The mechanism of oxidation of iron in sulfur dioxide atmosphere was studied by Wolter by means of ^{35}S radioisotope (Ref 17). Some reports have been made on high temperature corrosion of 9 to 12%Cr ferritic steel in simulated combustion gases with varying contents of SO_2 from 0 to 0.25% (Ref 18) as well as in air, flue gas, and steam (Ref 19). Hot corrosion behavior of modified 9Cr-1Mo steel in a mixture of coal-ash, alkali sulfates, and NaCl has been studied by Nateshan and Park (Ref 20).

Thus, it is clear from the above facts that very little work has been done so far to understand the mechanism of reaction of iron alloys exposed in SO_2 environment. Fe-Cr-Mo alloys are finding increasing application in many industries in particular in the systems exposed to multicomponent gaseous environment at elevated temperatures. The present work was undertaken to carry out systematic investigation on the effect of flow rate of sulfur dioxide and temperature of exposure, on corrosion behavior of 9Cr-1Mo steel in SO_2 environment.

2. Experimental

The material used in the present investigation was ferritic 9Cr-1Mo steel containing small amounts of Nb and V. The chemical composition of the steel is given in Table 1. Strips of

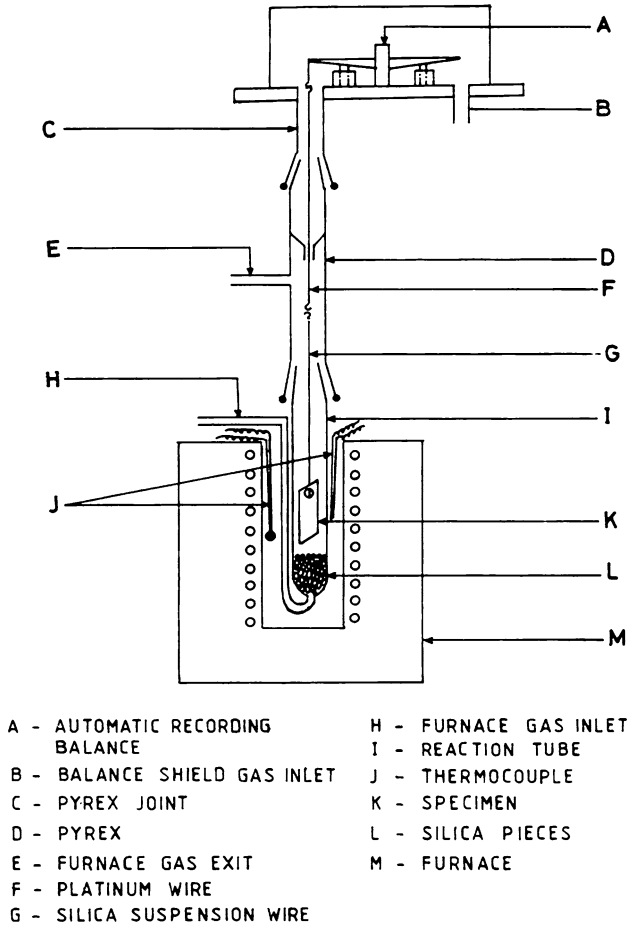

Fig. 1 Schematic diagram of the experimental set-up for corrosion

3 mm thickness of the 9Cr-1Mo steel were hot rolled at 1123 K to a thickness of 1.5 mm. The hot rolled strips were subjected to pickling in dilute H_2SO_4 and subsequently washed with water. The rough pickled surfaces were smoothened on belt grinder. Slightly oversized specimens ($20.5 \times 10.5 \times 1.5$ mm) were prepared. A hole of 1 mm diameter was drilled at one end of the specimen to facilitate its suspension in the reaction chamber. These specimens were mechanically polished on 400 grit emery paper and vacuum (1.33×10^{-1} Pa) sealed in silica tube then subjected to solution treatment at 1323 K for 30 min and cooled in furnace. The surface oxidized layer formed during annealing treatment was removed using belt grinding and final specimens of dimension $20 \times 10 \times 1$ mm were prepared. These specimens were mechanically polished on emery paper and subsequently on blazer cloth mounted on a polishing wheel, using suspension of alumina powder ($\approx$1 μm size) in water, as abrasive. The polished samples were thoroughly washed with distilled water following in acetone then weighed and measured for their dimensions before subjecting to sulfidation treatment.

A schematic diagram of the experimental set-up for studying corrosion behavior in SO_2 environment along with Cahn 1000 electro balance is shown in Fig. 1. The capacity of the balance was 100 g, and its sensitivity was 1 microgram. The weighing pan of the balance was attached to its one arm and the test specimen was hung from the other arm. The test specimens were suspended from the balance using platinum wire in the upper portion and quartz fiber in the lower reaction chamber. The reaction chamber consisted of two parts: the upper part made of Pyrex glass tube with 30 mm internal diameter and the lower part of transparent silica tube with 35 mm internal diameter. Chromel-Alumel thermocouple was positioned in the lower reaction chamber close to the specimen. A silica tube of 5 mm diameter, bent at right angles, was connected to bottom of the lower reaction chamber to allow flow of the reacting gas (SO_2) upward through bottom of the chamber.

The set-up had a tapered constrict in the Pyrex chamber and provision was made for flushing dry nitrogen in the balance chamber to check upward flow of SO_2 gas to prevent corrosive attack of sensitive parts of the balance. The lower portion of the reaction chamber was filled with silica chips, up to a height of about 50 mm, to cause uniform flow of SO_2 over the cross section of the reaction tube at the reaction temperature. A large number of sulfidation experiments were carried out and the results were found reproducible.

The flow of SO_2 gas was measured and controlled by capillary manometer using dibutyl phthalate as a monochromatic fluid which is inert to gaseous SO_2. The flow meter was calibrated by measuring the displacement of soap bubble in a graduated burette.

The weight gain as a function of the period of exposure was automatically recorded. The surface morphology of the scales formed from corrosion in SO_2 was examined by SEM (JEOL 840A) and the different phases in the scale were characterized by XRD (Rigaku D Max III C). The distribution of different elements in the scale was examined by EDAX (EDAX-711 B) attached to SEM (Phillips, PSEM 501) and EPMA (CAMECA).

3. Results

The effect of flow rate of SO_2 on corrosion behavior of 9Cr-1Mo steel at of 973, 1073, and 1173 K is presented in this section. The weight gain and morphological features of the scales, resulting from corrosion in SO_2 environment at different flow rates and temperatures are presented.

3.1 Effect of Flow Rate on Corrosion

In order to examine the effect of flow rate from 8.33×10^{-7} to 33.33×10^{-7} m^3/s of SO_2 at 1173 K, the weight gain was recorded for 6 h at each flow rate. This corresponds to linear flow rates of approximately 8.66×10^{-4} to 34.66×10^{-4} m/s in the reaction zone. The weight gain displayed by Cahn balance as a function of time is shown in Fig. 2. The weight gain as a function of square root of time is shown in Fig. 3. The linear behavior of the plot in Fig. 3 suggests that parabolic rate law was obeyed. The parabolic rate constants derived from these data are plotted as a function of flow rate at 1173 K (Fig. 4). The rate constants may be noted to be independent of flow rates within the range of flow rates investigated. In all subsequent experiments, the flow rate was maintained at 16.66×10^{-7} m^3/s, unless otherwise stated.

3.2 Effect of Temperature on Corrosion Behavior

Corrosion behavior of the annealed 9Cr-1Mo steel was investigated in SO_2 environment at 1 atmospheric pressure at a constant flow rate of 16.66×10^{-7} m^3/s for a fixed duration of 6 h, at three different temperatures of 973, 1073 and 1173 K. The variation of weight gain per unit area with duration of exposure is shown in Fig. 5. The variation of weight gain per

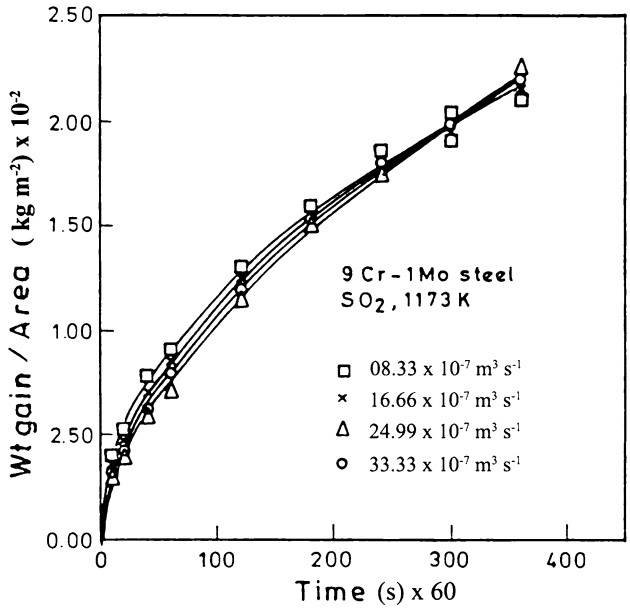

Fig. 2 Weight gain vs. time plots for different flow rates of SO_2 for corrosion of 9Cr-1Mo steel at 1173 K

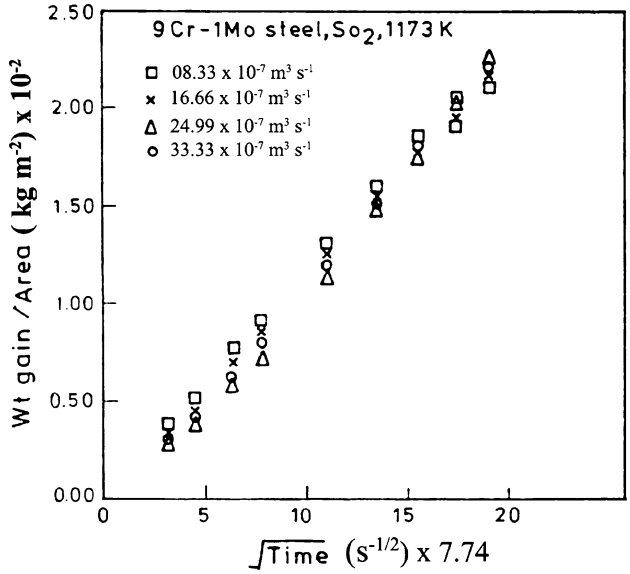

Fig. 3 Weight gain vs. $(time)^{1/2}$ plots for different flow rates of SO_2 for corrosion of 9Cr-1Mo steel at 1173 K

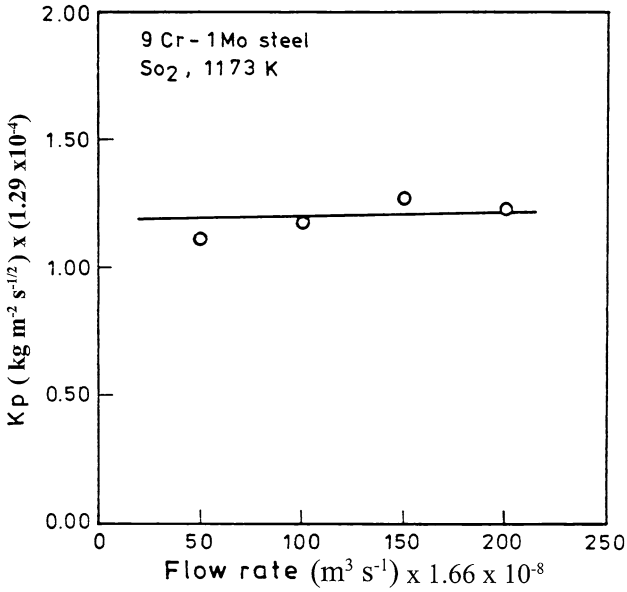

Fig. 4 Variation of parabolic rate constant (K_p) with flow rates of SO_2 for corrosion of 9Cr-1Mo steel at 1173 K

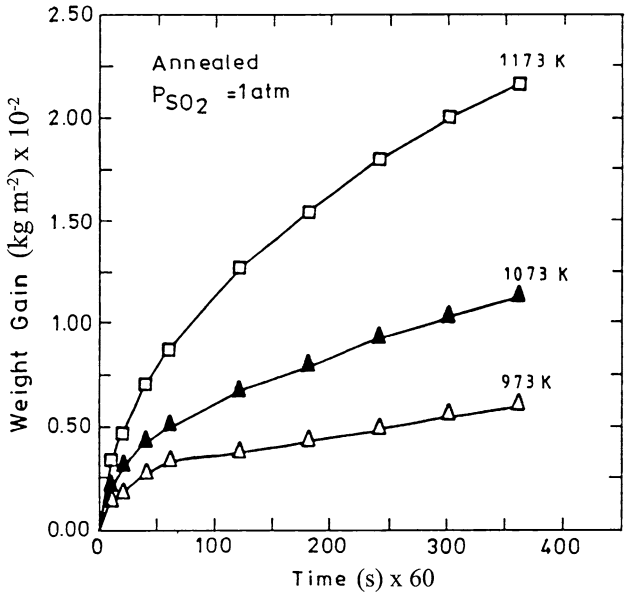

Fig. 5 Weight gain vs. time plots for corrosion of 9Cr-1Mo steel at various temperatures in SO_2 environment

unit area with exposure shows straight line behavior on double logarithmic scale (Fig. 6) at all the temperatures, and the average slope is ≈0.5 (Table 2). This indicates a parabolic rate law which was confirmed from linear plot of the weight gain/area versus $(\text{time})^{1/2}$ (Fig. 7). The rate constant (K_p), corresponding to different temperatures, is recorded in Table 3.

The activation energy for the process of corrosion was determined from the slope of Arrhenius type of plot between log (K_p) and 1/T (Fig. 8) and was estimated to be 16.4 ± 0.9 kcal/mol (Table 4).

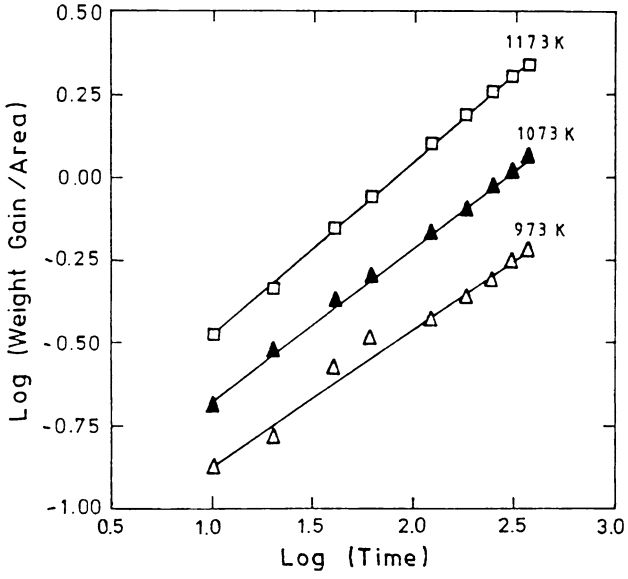

Fig. 6 Log-log plots of weight gain vs. time plots for corrosion of 9Cr-1Mo steel at different temperatures in SO_2 environment

Table 2 Values of *n* for corrosion of 9Cr-1Mo steel at p_{SO_2} = 1 atm

Temperature (K)	'*n*'
973	0.41 ± 0.02
1073	0.46 ± 0.08
1173	0.53 ± 0.05

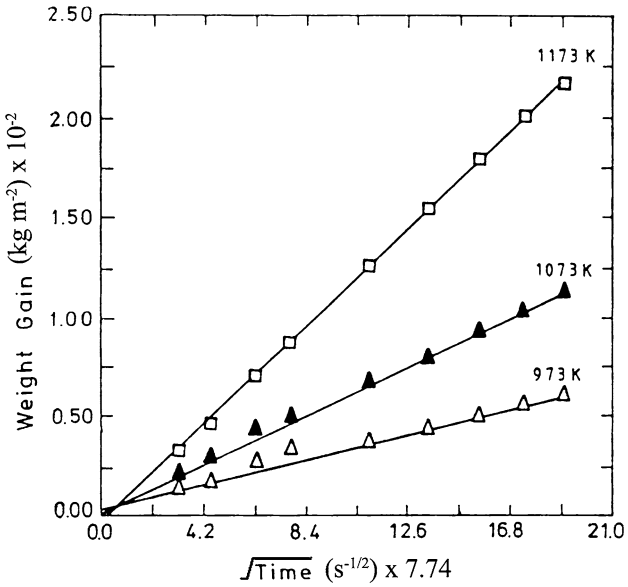

Fig. 7 Weight gain vs. $(\text{time})^{1/2}$ plots for corrosion of 9Cr-1Mo steel at different temperatures in SO_2 environment

3.2.1 Characterization of Scales Formed at Different Temperatures. The scales formed at different temperatures were characterized by XRD, EDAX, and EPMA techniques.

3.2.2 Characterization of Scale Formed at 973 K. The x-ray diffraction pattern of the exposed sample revealed that corrosion products were iron oxide, chromium oxide and chromium sulfide. Typical x-ray pattern from the scale formed at 973 K is shown in Fig. 9. Its surface morphology is shown in Fig. 10.

3.2.3 Characterization of Scale Formed at 1073 K. The x-ray diffraction pattern of the scale formed at 1073 K showed the presence of corrosion products identical to that formed at 973 K (Fig. 9). Surface morphology of the scales formed at 1073 K is shown in Fig. 11. The scale shows a dual phase type of structure with dark and bright contrast. There was appreciable growth of nodular phase with bright contrast. Further, it may be noted that volume fraction of the bright phase was considerably higher than that observed at the lower temperature of 973 K (Fig. 10). Also the distribution of the bright phase in the scale, formed at 1073 K, was more uniform than that formed at 973 K. At this temperature the scale was found to be intact and adherent.

3.2.4 Characterization of Scale Formed at 1173 K. The x-ray diffraction pattern of the sample exposed at 1173 K also showed that the corrosion products formed were iron oxide, chromium oxide and chromium sulphide, identical to that formed at 973 K (Fig. 9). However, the morphology of the scale formed at the highest temperature of 1173 K was totally different from those developed at lower temperatures of 973 and 1073 K. Figure 12(a) shows that outer layer of the scale was non-adherent and had tendency to peel-off. The bright regions, in four quadrants of the SEM micrograph in Fig. 12(a), show intact portion of the scale. The dark region between the bright areas showed underlying substrate of the scale, following spalling of the outer scale from these regions. Surface features of intact portion of the scale showed nodular features and fine cracks in the scale (Fig. 12b). This figure also shows preferential segregation of bright phase at grain boundaries. The morphology of the peeled off region is shown in Fig. 12(c). It may be noted that there are clear differences between the morphology of the intact scale (Fig. 12b) and the substrate (Fig. 12c). While there were nodular features on the intact scale, there were sharp acicular features on the substrate. Further, in contrast to the presence of fine cracks in the outermost intact scale, the inner scale was relatively free from such cracks.

Table 3 Values of K_p for corrosion of 9Cr-1Mo steel at p_{SO_2} = 1 atm

Temperature (K)	K_p (kg m^2 s$^{1/2}$) × 10^{-6}
973	29.28 ± 1.84
1073	73.14 ± 1.12
1173	151.96 ± 1.35

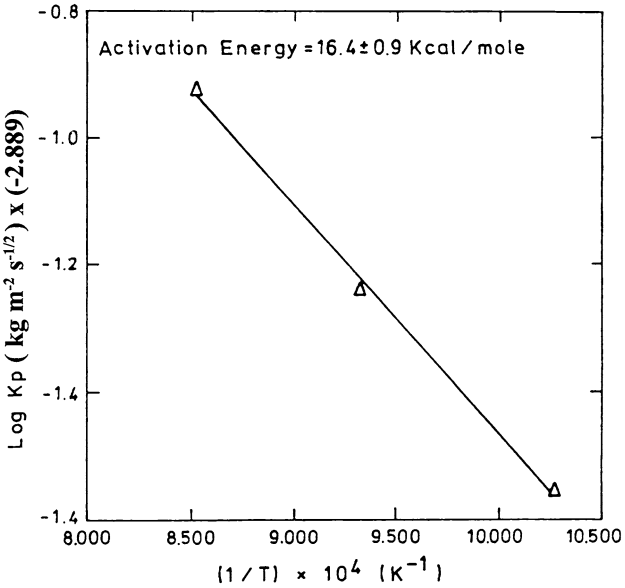

Fig. 8 Arrhenius plot for corrosion of 9Cr-1Mo steel in SO_2 environment

4. Discussion

Flatley and Birks (Ref 8) reported that the rate of scaling in Ar + SO_2 mixtures obeyed linear kinetics and was found to be a strong function of flow rate, up to a critical flow rate of

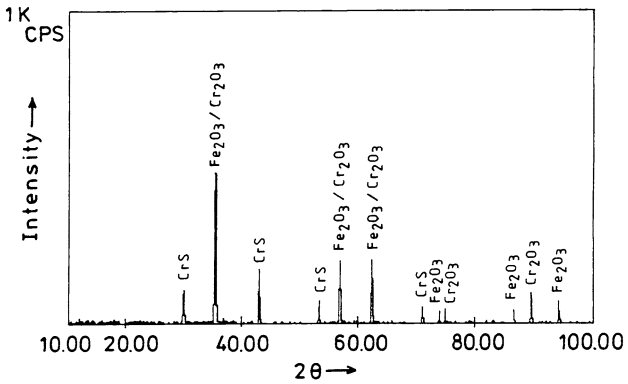

Fig. 9 XRD profile showing peaks of different compounds formed from corrosion of 9Cr-1Mo steel in SO_2 environment at 973 K for 6 h

Table 4 Activation energies for corrosion of iron and its alloys in sulfur dioxide atmosphere

Materials	Conditions	Activation energies	Reference
Fe + 0.07%C + 0.02% other	Ar + SO_2	16.29 ± 2.26	34
Pure Fe	S_{O_2}: 1 atm	52.59 ± 7.70	35
HSLA-R steel	S_{O_2}: 1 atm	49.34 ± 7.77	30
9Cr-1Mo steel	S_{O_2}: 1 atm	16.40 ± 0.90	Present work

16.66×10^{-7} m^3/s, at $p_{SO_2} = 20 \times 10^{-3}$ atm. As the SO_2 pressure was increased, linear rates were observed for smaller duration and subsequently parabolic rate law was obeyed. They have also reported that at $p_{SO_2} > 20 \times 10^{-3}$ atm the rates were independent of flow rates. Later, Tripathi (Ref 21) reported that the rate of corrosion of low alloy steel was independent of flow rate of sulfur dioxide within the range of 10.83×10^{-7} to 43.33×10^{-7} m^3/s at 1073 K. Thus, the results obtained in the present investigation on the kinetics of scale formation and the effect of flow rate of SO_2 are in agreement with those of the earlier investigations (Ref 8, 21). The values of activation energies reported by other investigators for corrosion of iron and its alloys in sulfur dioxide atmosphere are included in Table 4.

The morphology of scales examined under SEM is shown in Fig. 10. The scales appear to be heterogeneous and show coarse aggregates as well as fine nodular particles with bright contrast, in the predominantly dark matrix. It may be noted that number density of the fine nodular particles is considerably lower in peripheral region of the coarse and bright aggregates. It appears that the nodular particles nucleated from the sub-surface and grew toward outer surface of the scale.

The elemental analysis of the scale was carried out at various locations (Fig. 13) using EDAX. Scanning of the complete surface of the scale showed average Fe/Cr ratio varying from 13 to 14 (Fig. 13a). The Fe/Cr ratio at top of the large nodular particles, on ether side of the central region in Fig. 13(b) was found to be 22.4. The central region in Fig. 13(b) shows features of a cracked nodular particle of large size without the top surface with significant differences in the morphology from periphery to the center. The Fe/Cr ratio of the coarse particles (Fig. 13c) was found to be 17.2. However this ratio (Fe/Cr) was much lower (6.8-7.5) in the region between the coarse nodular particles, the dark region in the center in Fig. 13(d) suggesting substantial amount of Cr in this region.

The distribution of different elements across cross-section of the specimen, corroded in SO_2 environment at 973 K, may be seen from EPMA mapping of the elements in Fig. 14. The qualitative EPMA concentration line profiles of different elements across the scale/alloy interface of 9Cr-1Mo steel, following corrosion in SO_2 environment at 973 K for 6 h is shown in Fig. 15. It may be suggested, that outer layer of the scale with light contrast, was essentially of iron oxide, with small amount of chromium oxide. Whereas, the inner layer with

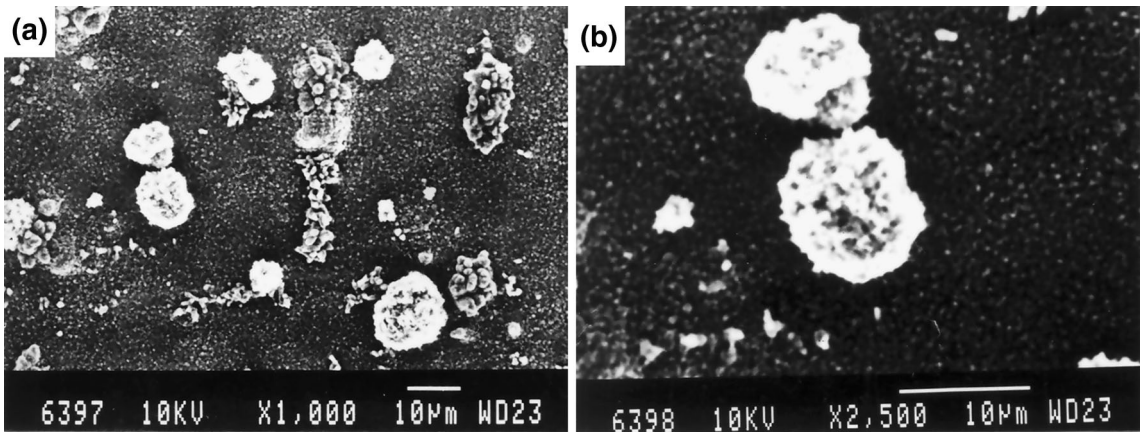

Fig. 10 SEM micrographs at different magnifications showing morphology of scale on 9Cr-1Mo steel formed by corrosion in SO_2 environment at 973 K for 6 h

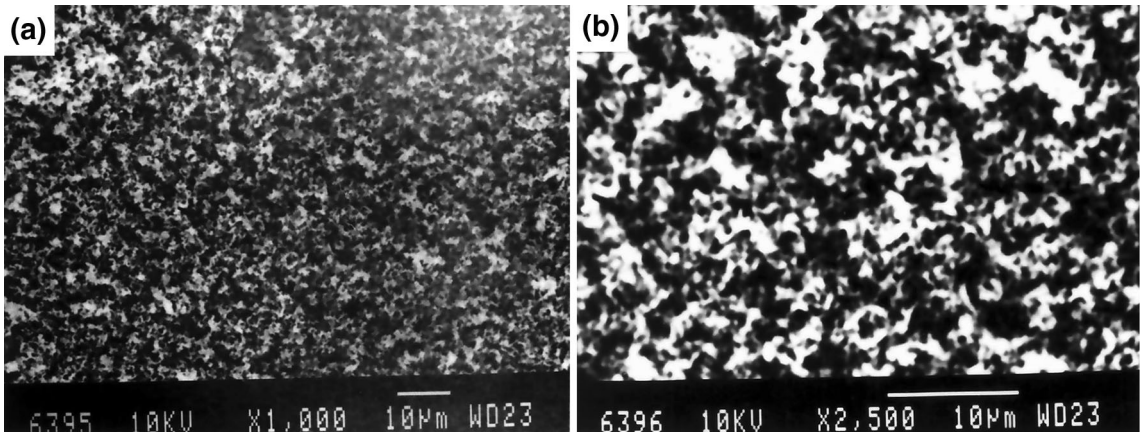

Fig. 11 SEM micrographs at different magnifications showing morphology of scale on 9Cr-1Mo steel formed by corrosion in SO_2 environment at 1073 K for 6 h

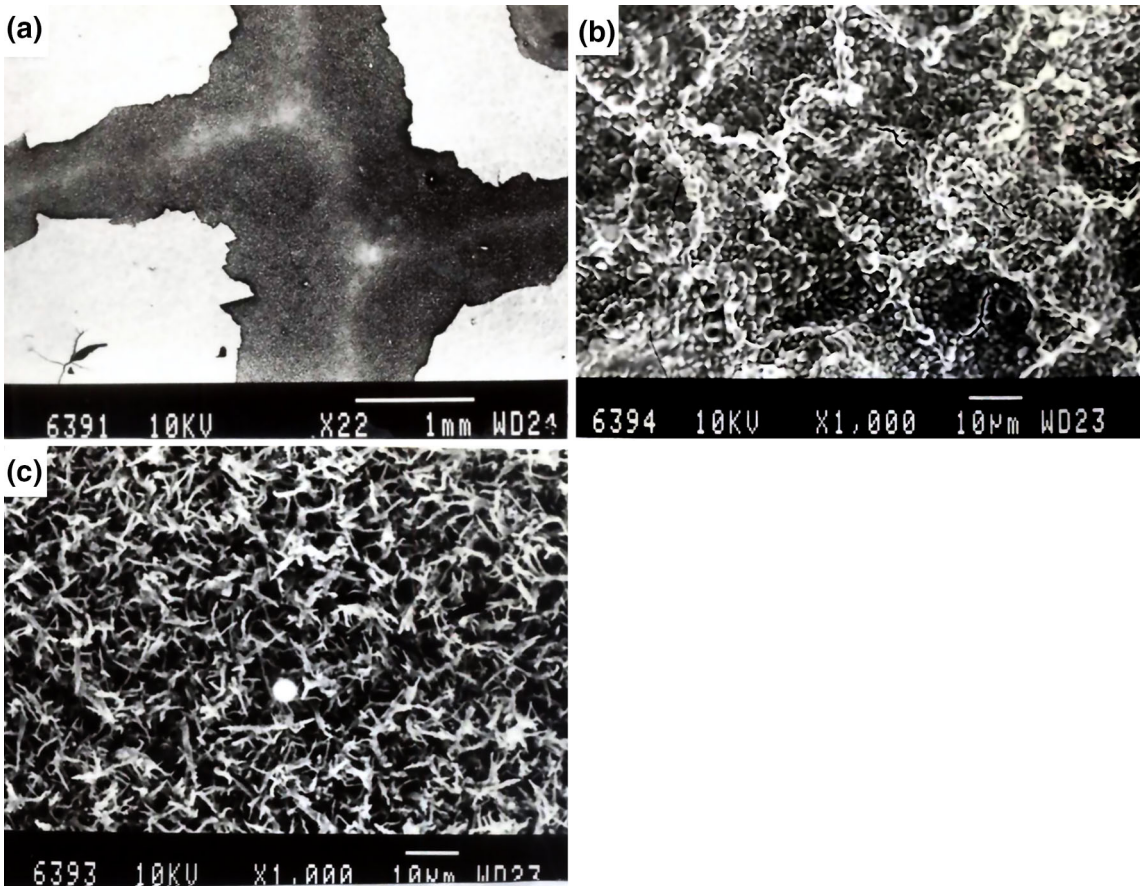

Fig. 12 SEM micrographs showing of morphology of scale formed by corrosion of 9Cr-1Mo steel in SO_2 environment at 1173 K for 6 h: (a) intact and peeled off scale, (b) magnified view of intact scale, (c) magnified view of pealed off scale

relatively dark contrast and irregular interface was predominantly of chromium sulfide and chromium oxide.

The cross section of the sample exposed to SO_2 environment at 1073 K for 6 h shows composite nature of the scale. The interface between the inner scale and the base material was quite complex as seen from EPMA mapping of the various elements (Fig. 16). The qualitative EPMA concentration line profiles of different elements across the scale/alloy interface of 9Cr-1Mo steel, following corrosion in SO_2 environment at 1073 K for 6 h, is shown in Fig. 17. It appears that outer layer of the scale was essentially of iron oxide and the inner layer was mainly of chromium sulfide containing some chromium oxide. It may also be seen from localized concentration of chromium and sulfur (Fig. 16) below inner layer of the scale, that there is a tendency for internal sulfidation of chromium. However, there was no evidence of internal sulfidation at the lower temperature of 973 K (Fig. 14).

Analysis of the elements in the scale was carried out along the lines shown in Fig. 18. The Fe/Cr ratio obtained from EDAX analysis showed very high and nearly comparable values both from the intact (Fig. 18a) as well as peeled of regions of the scale (Fig. 18b). However, the Fe/Cr ratio in the interior of the grains in the intact scale with dark contrast was found to be low (≈10), suggesting the presence of chromium (Fig. 18c). EPMA analysis of cross-section of the sample exposed to SO_2 environment at 1173 K for 6 h (Fig. 19) shows multilayers in contrast to double layers of the scales formed at 973 and 1073 K. Further, it may be inferred from Fig. 19 that outer-most thick layer of the scale consisted of iron oxide, followed by thin substrate of chromium sulphide, iron sulfide/iron oxide and chromium sulfide/chromium oxide and possibly iron sulfide/iron oxide. These observations suggest that the mechanism of growth of scales formed at these three temperatures was most likely to be the same.

A parabolic rate law of oxidation/corrosion indicates operation of the process through diffusion controlled mechanism. However, the small activation energy of 16.4 ± 0.9 kcal/mol does not support involvement of lattice diffusion of either cations or anions in influencing the rate. Gas boundary layer diffusion, which generally occurs with small activation energy, can also be ruled out because of negligible dependence of rate on flow rate of the reactive gas. Therefore, in order to obtain some information on the mechanism of formation of scales one therefore has to look critically into the microstructural details along with elemental distribution in the scales formed.

It is evident from EPMA study of the 9Cr-1Mo steel corroded in SO_2 environment (p_{SO_2} = 1 atm) at 1073 K for 6 h that the scale comprised of four distinct regions (Fig. 11). The top layer consisted of higher oxides of iron; the thin region below it had mixture of solid solution of chromium oxide and iron oxide. The region below the above one was thicker and consisted of a mixture of Cr_2O_3 and CrS and traces of FeS in its

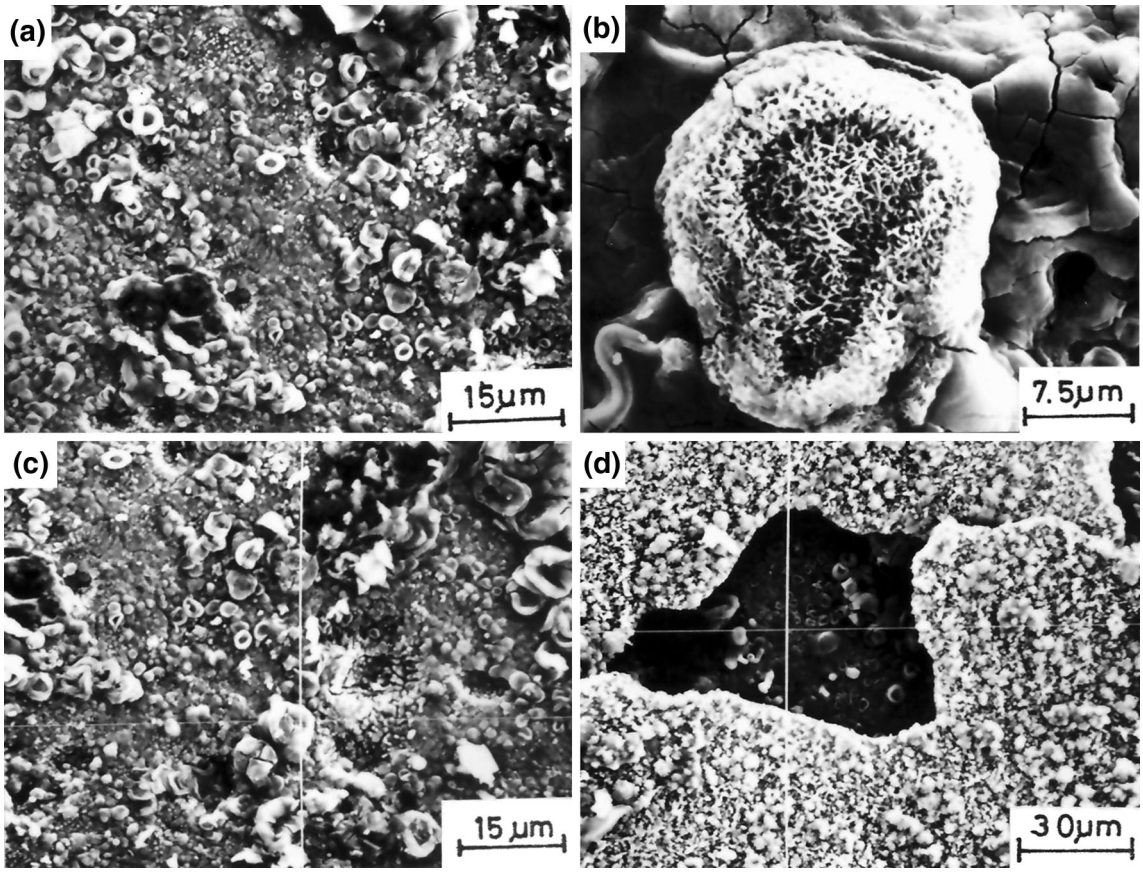

Fig. 13 SEM micrographs of different scales formed by corrosion in SO_2 environment at 973 K for 6 h, for determination of Fe/Cr ratio by EDS in different regions of scale

lower portion. The bottom most region at the scale/alloy interface showed depletion of Cr and patches of CrS. The corrosion process of 9Cr-1Mo steel leading to formation of a composite type of scales described above may be explained on the basis of relative activities of the constituent elements, their reaction with SO_2, stability of the resulting phases and transport of the constituent elements and SO_2 through the scale, as described below.

The partial pressures of sulfur and oxygen, corresponding to dissociation of SO_2 at 1 atm. pressure, at different temperatures of 973, 1073 and 1173 K were calculated using the available thermodynamic data (Ref 22). These values are given in Table 5.

The occurrence of various phases in the scale may be understood from the superimposed thermodynamic stability diagrams of Fe-O-S and Cr-O-S systems, corresponding to 1000 K (Fig. 20). It is obvious that as long as the Cr activity was high, the Cr_2O_3 and CrS were the only phases expected to form before iron began to oxidize.

Thus, when the 9Cr-1Mo steel came in contact with SO_2 at 1073 K chromium reacted with SO_2 to form CrS and Cr_2O_3 at the alloy/gas interface, as per the reaction:

$$7Cr + 3SO_2 \rightleftarrows 3CrS + 2Cr_2O_3 \qquad \text{(Eq 1)}$$

The initial formation of CrS and Cr_2O_3 on the alloy surface is shown schematically in Fig. 21(a). It may be noted from Eq 1 that three moles of CrS are formed for every 2 moles of Cr_2O_3 once a thin layer consisting of adjacent aggregates of CrS and Cr_2O_3 was formed, the activity of chromium decreased from the alloy/scale interface to scale/gas interface. When it reached a critical value which was too low to form thermodynamically stable CrS but high enough to form Cr_2O_3 in preference to iron oxide, only Cr_2O_3 was expected to form as a corrosion product. Thus, further thickening of the scale took place by growth of Cr_2O_3 resulting from diffusion of chromium through chromium oxide/chromium sulfide layer and subsequent oxidation by SO_2. This eventually led to enveloping of the regions of CrS formed earlier by Cr_2O_3 and increasing the concentration of Cr_2O_3 in the upper potion of this scale. The thickening of this layer led to further fall of Cr activity at scale/gas interface and reached another critical value below which formation of Cr_2O_3 became thermodynamically unstable relative to the formation of iron oxide (Fig. 21b). This critical chromium activity can be estimated from the standard free energy change of the following reaction at 1073 K and it was estimated to be 4×10^{-7} (assuming Fe/FeO equilibrium oxygen pressure of 1.8×19^{-19} atm) (Ref 23).

$$3FeO + 2Cr = Cr_2O_3 + 3Fe \qquad \text{(Eq 2)}$$

Further growth of the scale was due to oxidation of iron, which diffused from alloy/scale interface through preformed initial layer of the scale, consisting of island of CrS in Cr_2O_3 and subsequently through predominantly Cr_2O_3 layer to the

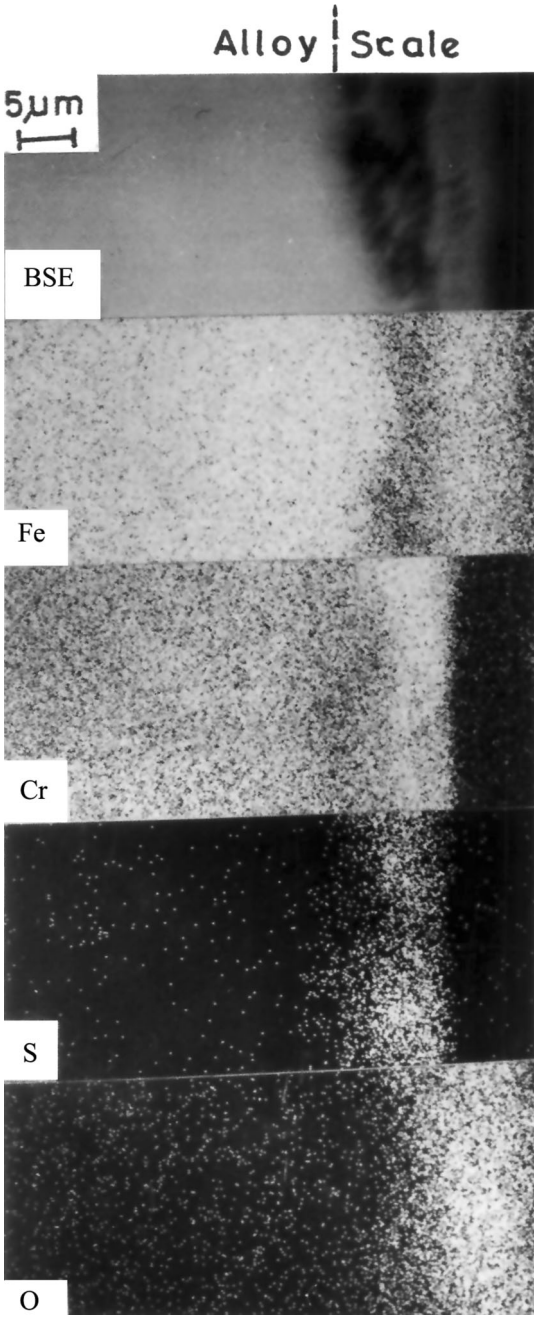

Fig. 14 EPMA x-ray maps of different elements in base material (9Cr-1Mo steel) and the scale formed by hot corrosion in SO_2 environment at 973 K for 6 h

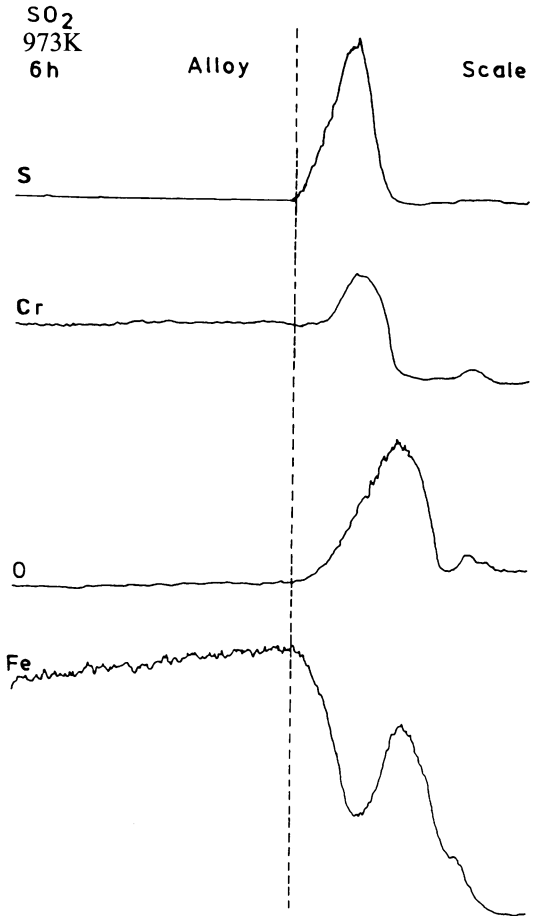

Fig. 15 Qualitative EPMA concentration line profile of different elements across the scale/alloy interface of 9Cr-1Mo steel after corrosion in SO_2 environment at 973 K for 6 h

scale/gas interface. At this stage corrosion products formed, as a consequence of reaction of iron with SO_2, will depend on the activity of iron at the scale/gas interface. The standard free energy change and activity of iron estimated for various possible reactions at 1073 K are presented in Table 6.

It can thus be seen that, as the activity of Fe got progressively lowered, the only stable corrosion product was expected to be higher oxides of Fe viz. Fe_3O_4 and Fe_2O_3. However, the x-ray diffraction study indicated the presence of only Fe_2O_3, which may be explained on the basis of its lower free energy of formation. Thus, subsequently above the Cr_2O_3 layer initially formation of iron oxide as well as sulfide was expected. However, if the activity of iron was too low to form iron sulfide, formation of only iron oxide was expected in the outermost region of the scale. Further, due to high temperature, wherever iron oxide was formed because of high mutual solubility of iron oxide and chromium oxide, formation of iron chromium spinel occurred in localized regions (Fig. 21c). Formation and growth of Fe_2O_3 thus occurred heterogeneously at favorable sites due to rapid transport of iron through the regions of iron-chromium spinel (Fig. 21d) (Ref 24).This process of the growth of Fe_2O_3 was evident from scanning electron micrographs of the samples corroded at 973 K in SO_2, showing varying sizes of nodules of Fe_2O_3 over the iron-chromium spinel and Cr_2O_3 scale (Fig. 10). The formation and growth of Fe_2O_3 at scale/gas interface was much faster at higher temperature i.e., at 1073 K (Fig. 11) as compared to that at 973 K (Fig. 10). The rate of growth of Fe_2O_3 increased with rise in temperature of exposure i.e., 1073 K due to increase in volume fraction of iron-chromium spinel and overall increase in the rate of transfer of iron through the scale. This heterogeneous growth of the scale at still higher temperature of 1173 K (Fig. 12) might led to formation of a continuous but porous Fe_2O_3 above the highly stressed underneath layer, resulting in eventual cracking and spalling of the scale. Spalling of the scale was also possible because of the presence of chromium sulfide

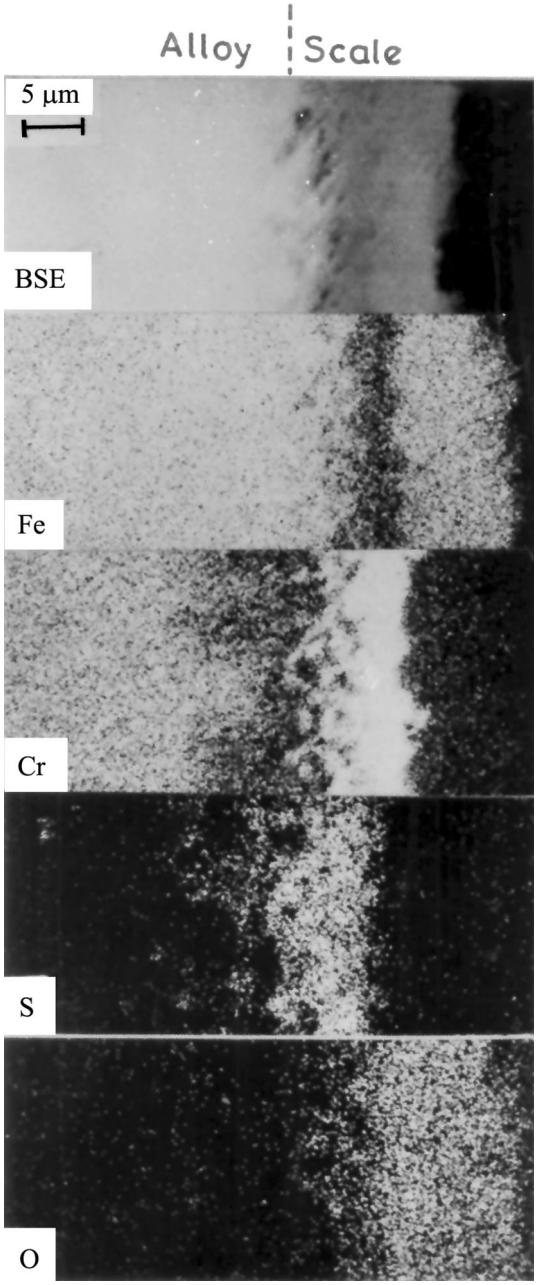

Fig. 16 EPMA x-ray maps of different elements in 9Cr-1Mo steel across the interface of base material and the scale resulting from hot corrosion in SO_2 environment at 1073 K for 6 h

either inside the alloy or at the scale/alloy interface. It has been suggested by Grabke et al. (Ref 25) that presence of sulfur at the alloy/scale interface promoted spalling of the scale. Sulfur may be present because of the transport of S_2/SO_2 from scale/gas interface to alloy/scale interface resulting in internal sulfidation of chromium. The possibility of formation of sulfide from internal sulfidation of the alloy (Fig. 21e) is discussed below.

Careful examination of the scanning electron micrographs and elemental distribution in the scales formed at 1173 K showed the presence of CrS, dispersed in substrate of the alloy/scale interface. CrS had also been found in the alloy matrix

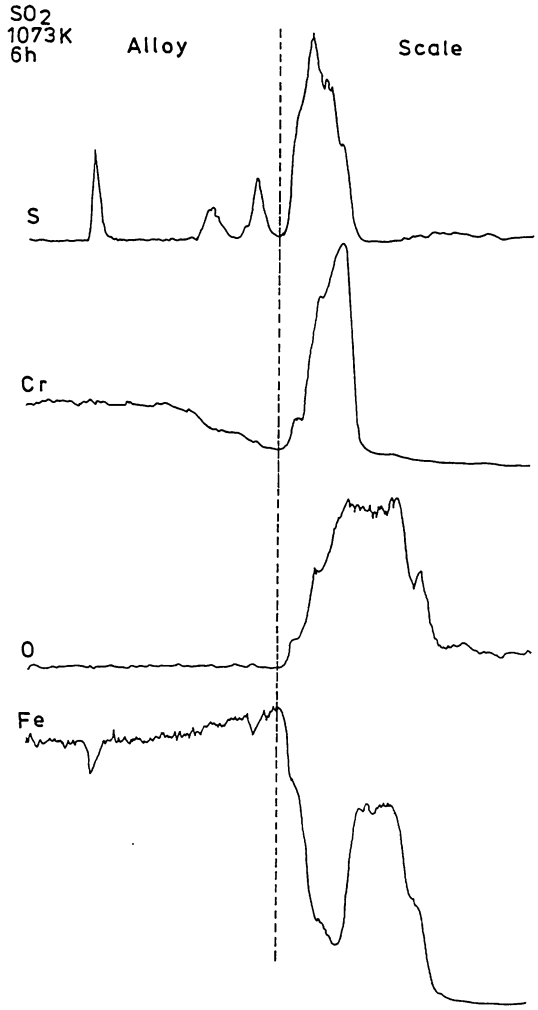

Fig. 17 Qualitative EPMA concentration line profiles of different elements across the scale/alloy interface of 9Cr-1Mo steel following corrosion in SO_2 environment at 1073 K for 6 h

preferentially along the grain boundary, suggesting internal sulfidation. Formation of internal sulfidised chromium might occur because of depletion of chromium and consequent prevention of external sulfide formation. The transfer of sulfur from gas/scale interface to scale/alloy interface for internal sulfidation might take place either through the lattice diffusion or through mechanical defects like pores, cracks, and/or grain boundary in the scale.

For the transfer of sulfur through compact Cr_2O_3 lattice there must be certain solubility of sulfur and Cr_2O_3. Lobnig et al. (Ref 26) have recently investigated solubility of sulfur in Cr_2O_3 at 973 and 1173 K and observed that solubility of sulfur in dense compact areas of the specimen was below detection limit of autoradiography, which was estimated to be better than 0.17 ppm. A number of investigators (Ref 11, 27-31) have established that permeation of sulfur through compact oxide scale can be considered to be negligible. The other mode of transfer of sulfur to the chromium depleted region could be by molecular transfer of SO_2 or S_2 (which can form via the reaction $4Fe + 3SO_2 = 2Fe_2O_3 + 3/2\ S_2$) taking place at scale/gas interface through cracks, pores, and/or grain boundaries in the scale. The SO_2 molecules could decompose on alloy/scale

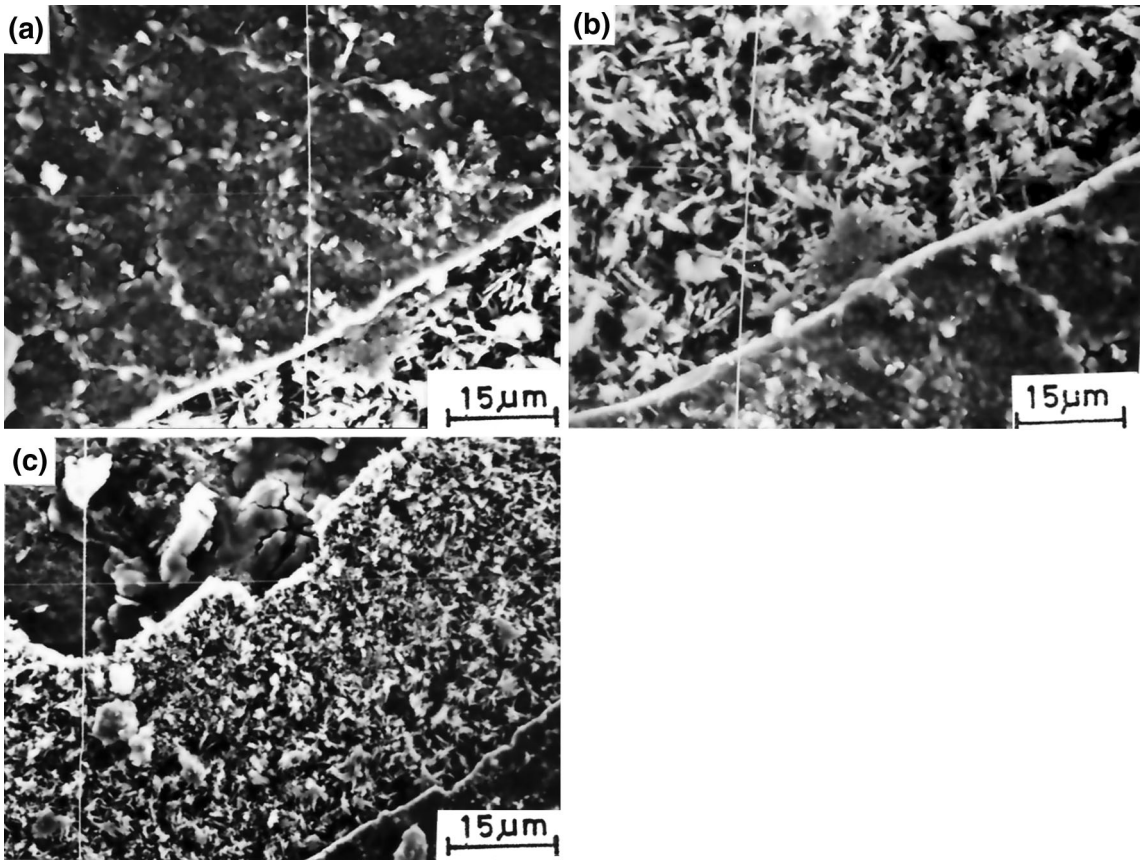

Fig. 18 EDAX analysis of Fe/Cr ratio in different regions of scale on 9Cr-1Mo steel, formed by corrosion in SO_2 environment at 1173 K for 6 h

interface to cause internal sulfidation even when sulfur pressure in gas atmospheres was lower than formation pressure of most stable sulfide in the system (Ref 6). Sulfidation from this process occurs due to development of high pressure of sulfur at the inner phase boundary as per the following equilibrium:

$$2SO_2 \rightleftarrows S_2 + 2O_2. \quad \text{(Eq 3)}$$

$$p_{S_2} = K\,(p_{SO_2}/p_{O_2})^2, \quad \text{(Eq 4)}$$

where oxygen partial pressure is expected to be very low because of metal/oxide equilibrium at the inner oxide/alloy phase boundary. Likewise, a very high thermodynamic activity of sulfur existed at inner phase boundary in case of nuclear transfer of SO_2/S_2 through the oxide layer (Ref 32). The process of internal sulfidation occurring because of molecular transfer of S_2 and SO_2 is schematically shown in (Fig. 22a and b) respectively.

The internal sulfidation leading to the formation of CrS caused depletion of Cr beneath the oxide scale and might initiate breakaway oxidation of the material. It has been postulated by Stringer (Ref 33) that a critical microstructure was attained by internal sulfidation and subsequent internal oxidation of the CrS to cause failure of oxide scale and breakaway oxidation, even at relatively low temperature. It may be noted that in present investigation there was little tendency for internal sulfidation at temperature of 973 K (Fig. 13). This was evident by the fact that conditions which favor internal sulfidation were low concentration of Cr, high solubility and diffusivity of sulfur in the alloy. It appears that a low temperature of 973 K was not be adequate to satisfy these conditions, at higher temperatures such a situation prevailed because of higher depletion of Cr due to higher rate of external oxidation and higher diffusivity because of higher activation energy of diffusion. Internal sulfidation was quite distinctly observed at higher temperature of 1073 K (Fig. 16). At still higher temperature of 1173 K (Fig. 18) there were distinct regions of oxide and sulfide resulting from internal sulfidation/oxidation.

In general, the process of scale formation due to corrosion of 9Cr-1Mo steel in SO_2 environment at these temperatures appears to be similar to that observed by Grabke et al. (Ref 25) during exposure of Fe-Ni-Cr alloy in coal gasification environments.

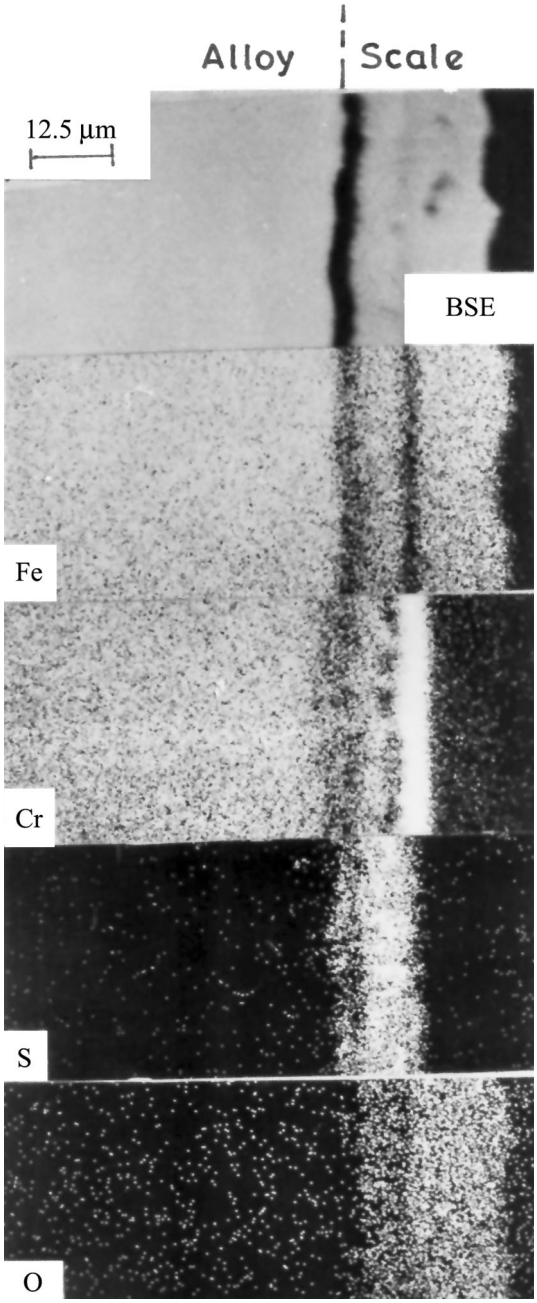

Fig. 19 X-ray maps from different elements from EPMA across the scale/alloy interface for 9Cr-1Mo steel following corrosion in SO_2 environment at 1173 K for 6 h

Table 5 Equilibrium partial pressure of sulfur (p_{S_2}) and oxygen (p_{O_2}) (for equilibrium reaction $2SO_2S_2 + 2O_2$ assuming $p_{O_2} = 2\ p_{S_2}$) in the temperature range 973 to 1173 K

Temperature (K)	p_{S_2}, atm	p_{O_2}, atm
973	2.21×10^{-11}	4.43×10^{-11}
1073	3.58×10^{-10}	7.16×10^{-10}
1173	3.61×10^{-9}	7.21×10^{-9}

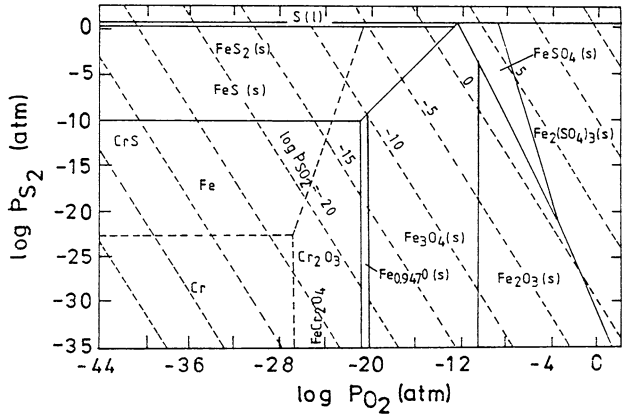

Fig. 20 Isothermal cross section of the simplified Fe-Cr-O-S phase diagram at 1000 K, formed by superimposition of the Fe-S-O and the Cr-S-O phase diagrams

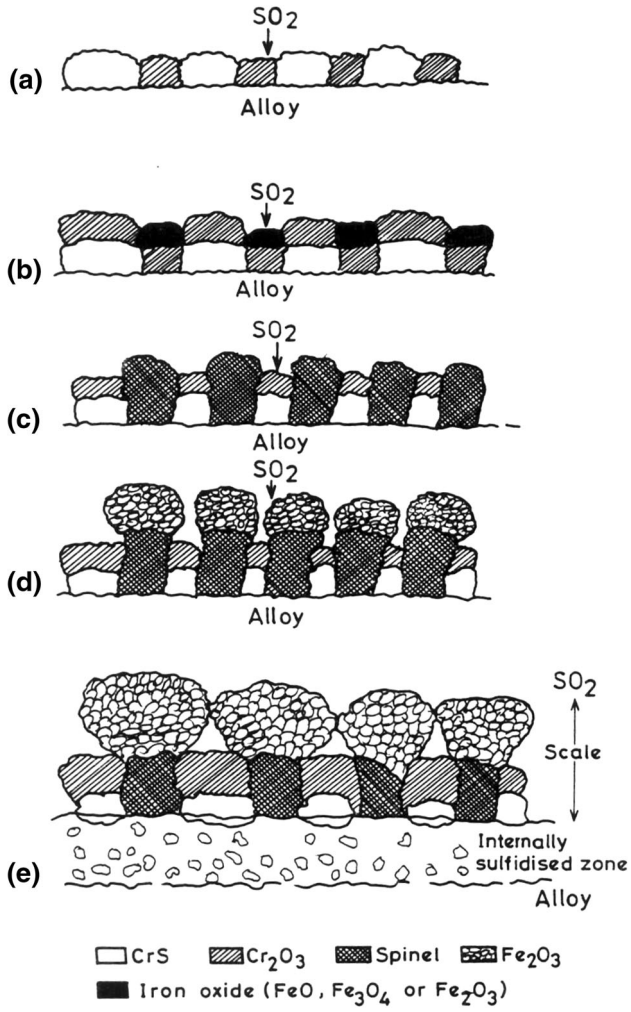

Fig. 21 Schematic diagram showing the sequence of formation of scale on 9Cr-1Mo steel exposed to SO_2 environment at 1 atm

Table 6 Activities of iron and standard free energy changes at 1073 K for various possible reactions

Reaction	Activity of iron (^{a}Fe)	$\Delta G°$, kcal
$Fe + SO_2 = FeS + O_2^*$	0.99	−45.18
$Fe + Fe_3O_4 = 4FeO$	0.55	−1.28
$3Fe + SO_2 = FeS + 2FeO$	6.24×10^{-4}	−47.52
$2Fe + SO_2 = 2FeO + ½ S_2^*$	1.24×10^{-5}	−25.16
$4Fe_2O_3 + Fe = 3Fe_3O_4$	2.35×10^{-7}	−32.76
$3Fe + 2SO_2 = Fe_3O_4 + S_2^*$	3.49×10^{-7}	−49.04
$4Fe + 3SO_2 = 2Fe_2O_3 + 3/2\ S_2^*$	3.66×10^{-7}	−57.18

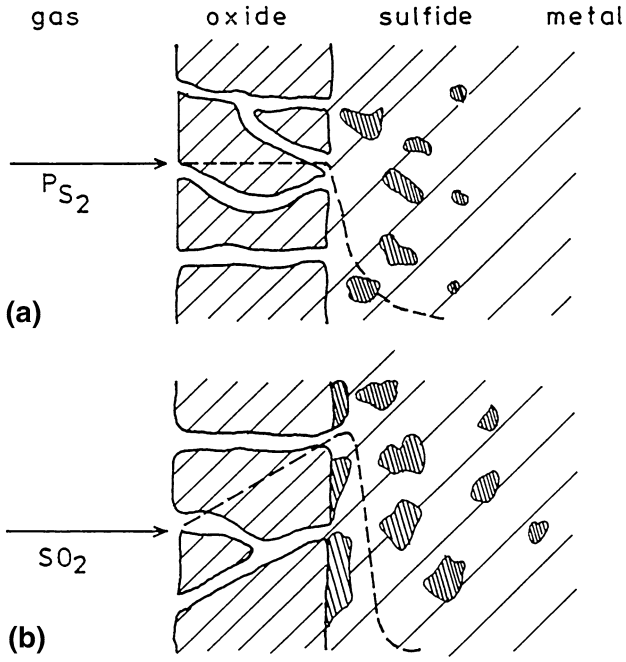

Fig. 22 Schematic diagram showing transfer of sulfur through defects in scale and internal sulphidation at elevated temperature in chromium depleted region by transfer of (a) elemental sulfur, (b) molecular sulfur

5. Conclusions

The following conclusions are drawn from this investigation.

1. Corrosion of annealed 9Cr-1Mo steel in annealed condition, in SO_2 environment, at 1173 K at different flow rates from 8.33×10^{-7} to 33.33×10^{-7} m^3/s, obeyed parabolic rate law and the rate constants are independent of flow rate in that range.
2. Corrosion of 9Cr-1Mo steel in SO_2 environment at constant flow rate of 16.66×10^{-7} m^3/s over a temperature range from 973 to 1173 K also followed parabolic rate law. However, the rate constants were dependent on test temperature.
3. The scale formed at 973 and 1073 K was of double layer type. The outer layer consisted essentially of iron oxide with small amount of chromium oxide. The inner region oxide scale contained essentially chromium sulfide and chromium oxide.
4. The tendency for internal sulphidation of Cr increased with temperature from 1073 to 1173 K.
5. A model is proposed for corrosion behavior of this steel in SO_2 environment at elevated temperature based on in depth characterization of the scales formed under different conditions, using various characterization techniques for the phases in the scale and distribution of different elements across the scale.

References

1. K.L. Luthra and W.L. Worrell, Simultaneous Sulfidation-Oxidation of Nickel at 603 °C in SO_2-O_2-SO_3 Atmospheres, *Metal. Mater. Trans. A*, 1979, **9**, p 621
2. R.A. Perkins, High Temperature Corrosion of Metals and Alloys in Coal Conversion Atmospheres, GOE, EPRI, GRI, NBS, *Third Annual Conference on Materials for Coal Conversion and Utilization*, October 10–15, U. S. Department of Energy, 1978
3. L.F. Grantham, P.H. Shaw, and R.D. Oldenkamp, Corrosion of Metals in Molten Mixtures of Alkali Metal Carbonates Containing Sulfur Compound, *High Temperature Metallic Corrosion of Sulfur and its Compound*, Z.A. Foroulis, Ed., The Electrochemical Society, Inc. New York, 1970
4. M. Hansen and K. Anderko, *Constitution of Binary Alloys*, 2nd ed., McGraw-Hill Book Co., New York, 1958
5. W.F. Chu and A. Rahmel, The Scaling of a Fe-20Cr Alloy in H_2-H_20-H_2S Mixtures, *High Temp. Mater.*, 1979, **4**, p 139
6. C.S. Giggins and F.S. Pettit, Corrosion of Metals and Alloys in Mixed Gas Environments at Elevated Temperatures, *Oxid. Met.*, 1980, **14**, p 363–413
7. A. Rahmel, The Scaling of Iron in Oxygen and Sulfur-Containing Gases, *Oxid. Met.*, 1975, **9**, p 401–408
8. T. Flatley and N. Birks, Oxidation of Iron in Atmospheres Containing Sulphur Dioxide, *J. Iron Steel Inst.*, 1971, **209**, p 523
9. P. Singh and N. Birks, Reaction of Cobalt in Ar-SO_2 Atmospheres at 500-900 °C, *Oxid. Met.*, 1978, **12**, p 23–34
10. M.R. Wootton and N. Birks, The Oxidation of Nickel in Atmospheres Containing Sulphur Dioxide, *Corros. Sci.*, 1972, **12**, p 829–836
11. G.J.W. Kor, The Diffusivity of Sulfur in Wüstite and its Solubility in Wüstite and γ Iron in Equilibrium with Each Other and a Liquid Oxysulfide, *Metal. Trans.*, 1972, **3**, p 2343–2347
12. G.H. Geiger and D.R. Poirier, *Transport Phenomena in Metallurgy*, Addison-Wesley Publishing Company, Massachusetts, 1973
13. F.S. Pettit, J.A. Goebel, and G.W. Goward, Thermodynamic Analysis of the Simultaneous Attack of Some Metals and Alloys by Two Oxidants, *Corros. Sci.*, 1969, **9**, p 903–910
14. B. Chatterjee and A.J. Dowell, High Temperature Reaction of Fe in SO_2, *Corros. Sci.*, 1975, **15**, p 639–648
15. A. Rahmel and J.A. Gonzalez, Scaling of Iron Between 700 and 900 °C in CO/CO_2 Mixtures with Minor Additions of COS, SO_2 and H_2S, *Mater. Corros.*, 1970, **21**, p 925
16. A. Rahmel and J.A. Gonzalez, Metallographic Investigations into the Structure of the Scale After Oxidation of Iron Between 700 and 900 °C in CO/CO_2 Mixtures with Minor Additions of COS, H_2S or SO_2, *Mater. Corros.*, 1971, **22**, p 283
17. J.G. Wolter, Study of Iron Oxidation in Sulfur Dioxide Atmospheres by Means of the ^{35}S Radioisotope, *Oxid. Met.*, 1977, **11**, p 81–90
18. K. Nakagawa, I. Kajigaya, T. Yanagisawa, M. Sato, and M. Abe, Study of Corrosion Resistance of Newly Developed 9-12%Cr Steels for Advanced Units, *Advanced Heat Resistance Steel for Power Generation*, R. Viswanathan and J.W. Nutting, Eds., Institute of Metals, London, UK, 1999, p 468
19. A. Fleming, R.V. Maskell, L.W. Buchanan, and T. Wilson, Material Developments for Supercritical Boilers and Pipework, *Materials for High-Temperature Power Generation and Process Plant Applications*, A. Strang, Ed., IOM Communications Limited, London, UK, 2000, p. 32
20. K. Natesan and J.H. Park, Fireside and Steam Side Corrosion of Alloys for USC Plants, *Int. J. Hydrog. Energ.*, 2007, **32**, p 3689–3697

21. B.D. Tripathi, PhD thesis, Banaras Hindu University, 1981
22. O. Kubaschewski and B.E. Hopkins, *Oxidation of metals and alloys*, 2nd ed., Butterworths, London, 1962, p 255
23. R.P. Salisbury and N. Birks, Oxidation of Iron-Chromium Alloys in Sulphurous Atmospheres, *J. Iron Steel Inst.*, 1971, **7**, p 534
24. H.J. Grabke, J.F. Norton, and F.G. Casteels, *High Temperature Alloys for Gas Turbine and Other Applications: Part I*, W. Betz, R. Brunetard,et al., Eds., D. Reidel, Dordrecht, 1986, p 245
25. H.J. Grabke, G. Kurbatov, and H.J. Schmutzler, Segregation Beneath Oxide Scales, *Oxid. Met.*, 1995, **43**, p 97–114
26. R.E. Lobnig, H.J. Grabke, H.P. Schmidt, and K. Hennessen, Sulfur in Chromia, *Oxid. Met.*, 1993, **39**, p 353–370
27. A. Rahmel, Kinetic Conditions for the Simultaneous Formation of Oxide and Sulphide in Reactions of Iron with Gases Containing Sulphur and Oxygen or Their Compounds, *Corros. Sci.*, 1973, **13**, p 125–136
28. M.C. Pope and N. Birks, Sulfur Solubility in NiO and CoO at 1000 °C, *Oxid. Met.*, 1978, **12**, p 191–204
29. G.J.W. Kor and E.T. Turkobgan, Sulfides and Oxides in Fe-Mn Alloys: Part II. Precipitation of Solid Sulfides and Liquid Oxysulfides During Oxidation of Iron Alloys, *Metall. Mater. Trans. B*, 1971, **2**, p 1571–1578
30. J.B. Wagner, *Defects and Transport in Oxides*, M. Seltzer and R. Jaffec, Eds., Plenum Press, New York, 1974, p 283
31. D.R. Chang, R. Nemoto, and J.B. Wagner, The Diffusion of Sulfur-35 in NiO, *Metall. Mater. Trans. A*, 1969, **7**, p 803–806
32. H.J. Grabke, *High Temperature Materials Corrosion in Coal Gasification Atmospheres*, J.F. Norton, Ed., Elsevier Applied Science, Amsterdam, 1984, p 59
33. J. Stringer, *Sulphidation as an Industrial Problem and a Limiting Factor*, Presentation at the Workshop on 'The high Temperature Corrosion of Alloys in Sulfur Containing Environments', 12/13, December, Patent, 1985
34. G.C. Wood and J. Boustead, The influence of group IIIA metals on the oxidation of Fe-Cr alloys, *Corros. Sci.*, 1968, **8**, p 719–723
35. T.K. Ross, The distribution of sulphur in corrosion products formed by sulphur dioxide on mild steel, *Corros. Sci.*, 1965, **5**, p 327–328